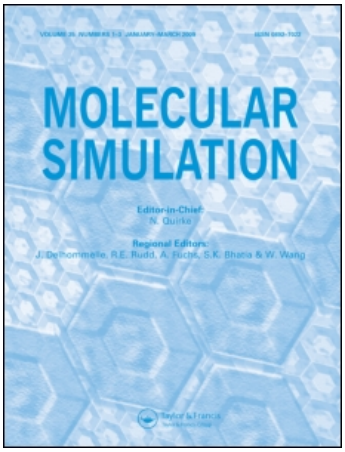

Molecular Simulation

Publication details, including instructions for authors and subscription information:
http://www.informaworld.com/smpp/title~content=t713644482

Diffusivities of Ar and Ne in Carbon Nanotubes

David M. Ackerman[a]; Anastasios I. Skoulidas[b]; David S. Sholl[c]; J. Karl Johnson[d]
[a] Department of Chemical and Petroleum Engineering, University of Pittsburgh, Pittsburgh, PA, USA [b] Department of Chemical Engineering, Carnegie Mellon University, Pittsburgh, PA, USA [c] National Energy Technology Laboratory, Pittsburgh, PA, USA [d] Department of Chemistry, Imperial College of Science Technology and Medicine, South Kensington, UK

Online publication date: 13 May 2010

To cite this Article Ackerman, David M. , Skoulidas, Anastasios I. , Sholl, David S. and Johnson, J. Karl(2003) 'Diffusivities of Ar and Ne in Carbon Nanotubes', Molecular Simulation, 29: 10, 677 — 684
To link to this Article: DOI: 10.1080/0892702031000103239
URL: http://dx.doi.org/10.1080/0892702031000103239

Molecular Simulation, Vol. 29 (10–11), October–November 2003, pp. 677–684

Diffusivities of Ar and Ne in Carbon Nanotubes

DAVID M. ACKERMAN[a], ANASTASIOS I. SKOULIDAS[b], DAVID S. SHOLL[b,c] and J. KARL JOHNSON[a,c,d,*]

[a]*Department of Chemical and Petroleum Engineering, University of Pittsburgh, Pittsburgh, PA 15261, USA;* [b]*Department of Chemical Engineering, Carnegie Mellon University, Pittsburgh, PA 15213, USA;* [c]*National Energy Technology Laboratory, Pittsburgh, PA 15236, USA;* [d]*Department of Chemistry, Imperial College of Science, Technology, and Medicine, South Kensington, SW7 2AY, UK*

(Received October 2002; In final form December 2002)

Atomically detailed simulations are used to compute the self-diffusivity and transport diffusivity of Ar and Ne through single walled carbon nanotube (SWNT) pores at room temperature. The diffusivities are computed over a range of loadings, corresponding to external equilibrium bulk pressures ranging from 0 to 100 bar. The diffusivities in carbon nanotubes are compared with diffusivities of the same gases in silicalite, a common zeolite, under the same conditions. We find that self-diffusivities are one to three orders of magnitude faster in carbon nanotubes than in silicalite, depending on loading. The transport diffusivities are about three orders of magnitude faster in nanotubes than in silicalite over all loadings studied. The equilibrium adsorption isotherms and computed diffusivities are used to predict fluxes through hypothetical membranes of nanotubes and silicalite. The fluxes for both Ar and Ne are predicted to be four orders of magnitude greater through nanotube membranes than through silicalite membranes of the same thickness.

Keywords: Argon diffusivity; Carbon nanotube membranes; Neon diffusivity; Silicalite membranes

INTRODUCTION

Diffusion of fluids in microporous materials has become an ever increasingly important topic over the past several decades. Catalytic and separation processes can depend critically on the diffusion characteristics of gases in sorbents such as zeolites [1–3], polymers [4–6] and nanoporous carbons [7,8]. Substantial progress has been made in developing new membrane materials and new synhesis techniques such that gas separation by organic or inorganic membranes is now commercially feasible [2,3]. However, wide-spread industrial use of membranes for separations is still seriously limited by a universal trade-off between the selectivity, or separation factor, and the permeability, or flux. The existence of an upper bound for the selectivity versus permeability was first quantified by Robeson some ten years ago [4]. The goal of developing a membrane with both high selectivity and high flux remains a major challenge today. In this paper, we present atomistic simulations of diffusion of two pure fluids, Ar and Ne, through single walled carbon nanotubes (SWNTs). The reason for examining SWNTs is that recent calculations by us have shown that these materials should exhibit extraordinarily high diffusivities for H_2 and CH_4 [9]. We use simulations to demonstrate that the diffusion of Ar and Ne through nanotubes of various diameters is orders of magnitude faster than diffusion of these same gases through silicalite, a commonly used zeolite for industrial applications with pores of about the same size as the nanotubes.

Two different pure-fluid diffusivities are of interest in both experiments and simulations. These are self- and transport diffusivity. Self diffusivity is the diffusion of a single tagged molecule through a fluid. Transport diffusivity relates the macroscopic flux of molecules in a system to a driving force in the concentration. The self-diffusion coefficient, D_s can be measured experimentally through incoherent quasi-elastic neutron scattering (QENS) and pulsed field gradient NMR [3,10]. Molecular simulations can be used to

*Corresponding author. E-mail: karlj@pitt.edu

ISSN 0892-7022 print/ISSN 1029-0435 online © 2003 Taylor & Francis Ltd
DOI: 10.1080/0892702031000103239

measure the self-diffusion coefficient through the Einstein relation,

$$D_s(c) = \lim_{t\to\infty} \frac{1}{6Nt} \left\langle \sum_{i=1}^{N} |\vec{r}_i(t) - \vec{r}_i(0)|^2 \right\rangle \qquad (1)$$

where c is the concentration or density, t is the time, N is the number of molecules in the system, and $\vec{r}_i$ is the vector position of molecule i. The transport diffusivity is defined by Fick's law of diffusion,

$$\vec{J} = -D_t(c)\nabla c \qquad (2)$$

where $\vec{J}$ is the flux, D_t is the transport diffusion coefficient, and ∇c is the gradient of the concentration. D_t is also known as the Fickian diffusion coefficient. The self- and transport diffusion coefficients depend on concentration in different ways in microporous solids and have different values except at zero concentration where they are equal [3]. Previous studies have shown that in zeolites and SWNT pores $D_s(c)$ decreases very rapidly with increasing concentration due to fluid–fluid collisions, whereas $D_t(c)$ typically increases with increasing concentration [9,11]. Values of D_t can be measured experimentally through coherent QENS [12] and macroscopic techniques such as permeation chromatography and sorption uptake [3]. Measurement of D_t from simulations is not as straightforward as for D_s. In addition, D_t is a collective property, depending on the motion of the entire fluid, while D_s is a single molecule property. Hence, the statistical accuracy of D_t is inherently much lower than for D_s. There are basically two classes of methods for computing D_t from molecular simulations (MD), one employs non-equilibrium molecular dynamics (NEMD) techniques while the second uses equilibrium molecular dynamics (EMD) methods. The most widely used NEMD method imposes a chemical potential gradient across some portion of a simulation cell or section of a membrane in order to measure the resulting flux of molecules. $D_t(c)$ is then inferred from Eq. (2). The concentration gradient is generated through dual control volume grand canonical MD (DCV-GCMD) [13–16]. The EMD method for computing $D_t(c)$, first developed by Theodorou and coworkers [17,18], proceeds by writing

$$D_t(c) = D_0(c)\left(\frac{\partial \ln f}{\partial \ln c}\right)_T, \qquad (3)$$

where $D_0(c)$ is called the corrected diffusivity [17,18] and f is the fugacity of the bulk fluid in equilibrium with the adsorbed phase at the given concentration c. The derivative term multiplying $D_0(c)$ is referred to as the thermodynamic correction factor and can be evaluated from the equilibrium adsorption isotherm calculated, for instance, from grand canonical Monte Carlo (GCMC). The corrected diffusivity can be computed from EMD using [11,17,19]

$$D_0(c) = \lim_{t\to\infty} \frac{1}{6Nt} \left\langle \left| \sum_{i=1}^{N} [\vec{r}_i(t) - \vec{r}_i(0)] \right|^2 \right\rangle. \qquad (4)$$

In this equation, $\langle\cdots\rangle$ indicates an average over multiple independent EMD trajectories each of which contain N mobile adsorbed molecules. One useful way to interpret this result is that $D_0(c)$ is related to the diffusive motion of the center of mass of the mobile molecules in the simulation volume. In practice, this average must be computed by performing at least 10–20 independent EMD simulations due to the inherently poorer statistics of Eq. (4) compared with Eq. (1). This means that computing the corrected diffusivity is intrinsically more demanding than computing the self-diffusivity. Given that the EMD method requires both multiple independent trajectories and an additional GCMC calculation in order to compute $D_t(c)$ one might suppose that DCV-GCMD is more efficient than EMD for computing $D_t(c)$. However, there are three advantages of the EMD over NEMD methods. First, non-equilibrium methods only give accurate results when used in regimes where linear response theory is valid, so tedious calculations may need to be performed to fully calibrate them [17]. Second, EMD methods make it possible to compute $D_0(c)$ and $D_s(c)$ directly from a single calculation, unlike non-equilibrium methods. Since there are long-standing controversies about correctly comparing experimental measurements of self- and transport diffusion [3,12,18,20,21], it is very useful to have data on both these quantities that can be compared unambiguously [11]. Third, for DCV-GCMD the concentration at which $D_t(c)$ should be evaluated is not well defined. In fact, DCV-GCMD is only able to give an average value for D_t, not the exact concentration dependence of $D_t(c)$.

In this work, we focus on diffusion in SWNTs. Carbon nanotubes were first discovered by Iijima as multi-walled structures consisting of concentric shells [22]. Single walled nanotubes were later isolated by both Iijima and Ichihashi [23] and Bethune *et al.*, [24] SWNTs have typical diameters on the order of 1 to 2 nm, although diameters as small as 0.4 nm have been reported [25–29]. SWNTs form ropes or bundles of individual nanotubes arranged on a hexagonal lattice with an inter-tube gap of about 0.32 nm [30]. These ropes are typically several microns in length, although recent claims of several centimeter have been made [31]. The diameter, helicity, and electronic properties of a SWNT are defined by the nanotube indices, (n, m) where n and m are integers [32]. These indices define how

the SWNT may be formed by mapping a graphene sheet to the surface of a cylinder. In this work, we will consider nanotubes defined by the indices (8,8), (10,10) and (12,12), having diameters of 1.085, 1.356 and 1.627 nm, respectively. We consider only defect free nanotubes in this study. Such nanotubes are atomically smooth, with no asperities on the inside of the nanotube, in contrast to zeolites, which have constrictions or windows in between wider channels. We will show that this inherent smoothness that leads to unparalleled diffusion rates in SWNTs.

There have been very few simulations of diffusion in carbon nanotubes. Nicholson studied transport selectivity of CH_4 and CO_2 in model cylindrical carbon pores, but with structureless walls so that wall-molecule collisions were modeled with a pure diffuse reflection algorithm [33]. Therefore, these results are not directly related to transport in SWNTs, because the transport coefficients are sensitive functions of the wall-fluid collision properties.

Mao and Sinnott [34–36] have studied the self-diffusion of pure methane, ethane and ethylene in a number of different SWNTs using MD. They have also studied diffusion of mixtures of methane/ethane, methane/n-butane and methane/isobutane in a number of different nanotubes. They have used a reactive empirical bond order potential [37–39] (REBO) to account for the short range reactive interactions (core–core repulsions and valence electron attractions). The long-range interactions were modeled with empirical Lennard-Jones (LJ) potentials, modulated to zero at short distances where the reactive potential is non-zero.

The REBO potential realistically accounts for the nanotube flexibility. The self-diffusion coefficients for methane at high pore loadings were found to be on the order of $10^{-4}\,cm^2\,s^{-1}$ This is in reasonable agreement with the values calculated in our previous work at the highest loadings [9].

Work by Sokhan and coworkers on simulated Poiseuille flow in graphitic slit pores and carbon nanotubes using NEMD is related to our work [40,41]. Their results show that the graphene structures, both slit pores and SWNTs, have very long hydrodynamic slip lengths, even for fluids that are very strongly adsorbed in the pores. This, they point out, is a direct consequence of the low degree of corrugation in the graphene structures. This result precisely agrees with our observations that diffusivities in SWNTs are much faster than other sorbents because of the inherent smoothness of the potential energy surface. Sokhan *et al.*, modeled the graphene planes and carbon nanotubes using the fully flexible Tersoff-Brenner potential [38,42,43].

Only one other group has attempted to determine the transport diffusivity of adsorbed gases in carbon nanotubes. Transport diffusion coefficients for CH_4/CF_4 mixtures in an isolated multiwalled carbon nanotube (MWNT) were computed from a series of DCV-GCMD simulations by Düren *et al.*, [44]. They used a model MWNT consisting of three concentric nanotubes with the innermost nanotube having a diameter of 2.978 nm. Single LJ spheres were used to model CH_4 and CF_4 and the pore walls were represented by atom explicit LJ potentials for each of the carbon atoms in the nanotube. However, instead of using the atom explicit pore walls to generate correct scattering trajectories, they used a thermal scattering algorithm developed for transport through model carbon membranes [45]. The thermal scattering algorithm assumes that molecules reach complete thermal equilibrium with the pore wall and are re-emitted in a random direction following a collision with the wall. Use of this algorithm drastically changes the diffusive behavior of the fluid because the diffusive transport is dictated by the details of the fluid-wall scattering events. As a result, the D_t values measured from their simulations are orders of magnitude smaller than those calculated from our previous work [9] and in this study. We emphasize that the low diffusivities observed by Düren *et al.*, are an artifact of a physically incorrect treatment of gas-nanotube collisions. This result underscores the importance of accurately accounting for the gas-solid interactions when computing diffusivities.

In our previous work [9], we have used atomistically detailed models of carbon nanotubes to compute the self- and transport diffusion coefficients from the EMD methods first proposed by Theodorou and coworkers [17,18]. We calculated $D_s(c)$ and $D_t(c)$ for H_2 and CH_4 at room temperature in a (10,10) nanotube and in two zeolites, namely, silicalite and ZSM-12. We also computed the equilibrium isotherms and found that these were quite similar for all three sorbents on a volumetric (moles m^{-3}) basis. The diffusion coefficients, however, were strikingly different in each of the three sorbents. The zero coverage self-diffusion coefficients for both H_2 and CH_4 are about three orders of magnitude larger in the (10,10) SWNT than in either silicalite or ZSM-12. Values of $D_s(c)$ decrease rapidly with increasing loading in all three sorbents, but the decrease of $D_s(c)$ in the SWNT is much more dramatic, so that at the highest loading studied D_s is only about one order of magnitude higher in the SWNT than in the zeolites. The transport diffusivity is roughly constant with increasing coverage for both sorbates in all three sorbents. Therefore, $D_t(c)$ remains about three orders of magnitude higher in the (10,10) SWNT than in the two zeolites over the entire range of concentrations. We also computed $D_s(c)$ and $D_t(c)$ for H_2 in the (6,6) nanotube, with a diameter of 0.81 nm, for comparison with the values obtained for the (10,10) SWNT, which has a diameter of 1.36 nm. We found that both D_s and D_t were larger in the (6,6) than in the (10,10)

nanotube for all concentrations studied. For example, the zero loading diffusivities are approximately 10 and $1\,cm^2\,s^{-1}$ in the (6,6) and (10,10) SWNTs, respectively. The increase in the diffusivity with decreasing diameter of the nanotube is due to the decrease in corrugation as the carbon atoms in the wall of the nanotube become closer together. This same sort of phenomenon was noted by Sokhan and coworkers, who observed shorter slip lengths when the density of wall atoms was reduced with respect to the graphene lattice [40,41].

In this paper, we present results for $D_s(c)$ and $D_t(c)$ of Ar and Ne in (8,8), (10,10) and (12,12) SWNTs over a range of pore loadings corresponding to bulk phase equilibrium pressures from 0 to about 100 bar. We compare our results to diffusivities of Ar and Ne in silicalite over the same pressure range. All calculations are at room temperature. We discuss the significance of these results in terms of hypothetical membranes that could be constructed from SWNTs.

SIMULATION METHODS

The potential models used in this study are all of the LJ form. The parameters are listed in Table I. The solid–fluid potentials were derived from the Lorentz-Berthelot combining rules,

$$\sigma_{ij} = \frac{\sigma_i + \sigma_j}{2}, \tag{5}$$

$$\epsilon_{ij} = (\epsilon_i \epsilon_j)^{1/2}, \tag{6}$$

where σ is the size parameter and ϵ is the energy parameter. The fluid parameters listed in Table I are those used by Skoulidas and Sholl [11] in their study of transport diffusivities in silicalite. The carbon parameters were developed for graphite [46]. We assume that the nanotubes are completely rigid, with all carbon atoms fixed in their ideal lattice positions. The solid–fluid potential was precomputed on a grid and Hermite cubic polynomial interpolation [47] was used to compute the potential and the forces during the simulation. The grid spacing was set to 0.02 nm. This is the same procedure used for computing isotherms and diffusivities in zeolites by Skoulidas and Sholl [11,19]. The fluid–fluid and solid–fluid potentials were truncated at a distance of 2 nm; no long-range corrections were applied.

TABLE I Lennard-Jones potential parameters for the atoms considered in this study

Atom	ϵ/k *(K)*	σ *(nm)*
Ne	35.7	0.2789
Ar	124.07	0.342
C	28.0	0.34

The solid–fluid interaction parameters were obtained from the Lorentz-Berthelot combining rules.

In this paper, we have computed $D_s(c)$ and $D_0(c)$ from the EMD method outlined above. Equations (1) and (4) were implemented within the EMD formalism. Simulations were started from configurations generated from GCMC simulations to achieve the desired loading, after which the configuration was relaxed within the canonical (NVT) ensemble using Monte Carlo, followed by NVT MD before data were collected. The system was typically equilibrated for 100 000 time steps, with a time step of 0.001 in reduced units. Fifteen or more different independent trajectories were typically generated, each with their own equilibration period, in order to improve the statistics of Eq. (4). Note that running a single long simulation with different time origins does not produce as accurate results as using independent trajectories. Different random number seeds were used to generate the initial configuration and the initial velocities for the independent trajectories. The length of the simulation cell was varied from 20 to 200 nm so that the number of molecules was typically between 80 and 300. Periodic boundary conditions were applied in the direction of the nanotube axis. The temperature was maintained through use of a Nosé-Hoover thermostat [48,49].

Once the $D_0(c)$ values were calculated, $D_t(c)$ values were computed from Eq. (3) using the thermodynamic correction factor. This factor was computed by generating the equilibrium isotherm and fitting the isotherm to a double Langmuir isotherm,

$$n = \frac{a_1 P}{a_2 + P} + \frac{b_1 P}{b_2 + P}, \tag{7}$$

where n is the loading, P is the pressure, and a_i and b_i adjustable parameters. The derivative needed in Eq. (3) was then computed from Eq. (7) using experimental second and third virial coefficients [50] to relate the pressure and the fugacity. The isotherms were computed from GCMC simulations [48,49] using the same potentials as for the EMD simulations. The probabilities of making displacements, creations, and deletions were set to 40, 30 and 30%, respectively. The GCMC simulations were equilibrated for 2×10^6 configurations, after which data were collected for 4×10^6 to 10^7 configurations, with longer simulations being used for the highest loadings.

RESULTS AND DISCUSSION

The equilibrium isotherms for Ar and Ne at 298 K in SWNTs and silicalite are shown in Figs. 1 and 2. The data were computed by assuming that the SWNTs form an ideal hexagonal array with an inter-tube gap of 0.32 nm, which corresponds to the close-packed

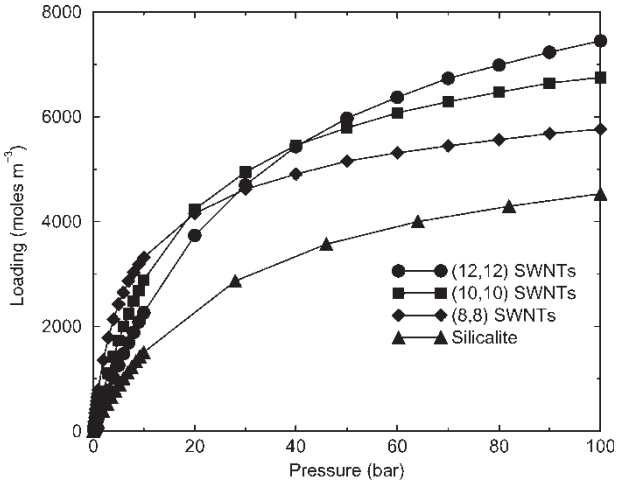

FIGURE 1 Adsorption isotherms for Ar at 298 K in arrays of (12,12) (circles) (10,10) (squares) and (8,8) (diamonds) SWNTs, and silicalite (triangles). The nanotubes are assumed to form a close-packed hexagonal structure. Silicalite is taken to be a perfect crystal. Lines are to guide the eye.

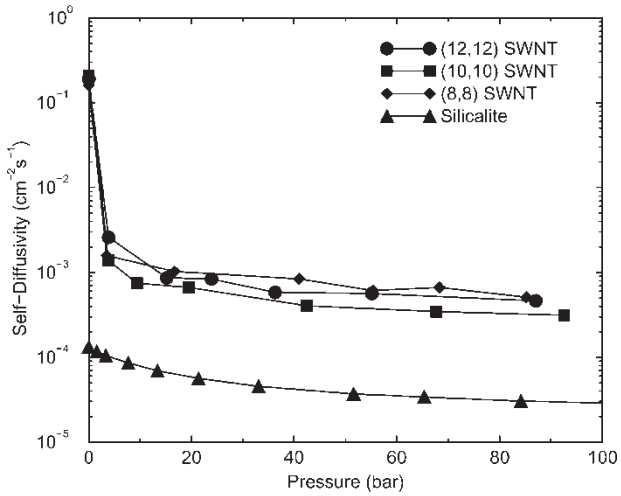

FIGURE 3 Self diffusivity of Ar at 298 K in (12,12) (circles) (10,10) (squares), and (8,8) (diamonds) SWNTs and silicalite (triangles).

structure [30], and that no fluid adsorbs in the interstitial channels. The silicalite isotherms assume a defect-free single crystal of the zeolite. Adsorption in the nanotubes and silicalite is comparable, but the amount adsorbed is always higher in the SWNTs we have studied. Note that for Ar the amount adsorbed at higher pressure decreases with decreasing diameter of the nanotube, whereas at low pressure (lower than 10 bar) the opposite trend is observed. This is evidence of the trade off between the stronger adsorption potential for the smaller nanotubes and the larger free volume available in the larger nanotubes. The adsorption of Ne in the nanotubes and silicalite is substantially weaker than Ar. This reflects the weaker solid–fluid interactions and lower critical temperature for Ne (i.e. Ne is at a much higher reduced temperature than Ar). There is little difference between the Ne isotherms in the (12,12), (10,10) and (8,8) nanotube arrays. This is because the amount adsorbed is dominated by the surface area, not the volume. Hence, in the larger nanotubes the increase in surface area is mostly offset by the increase in volume.

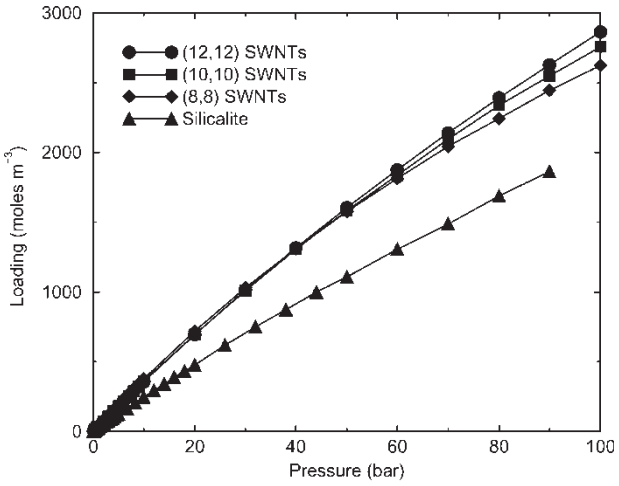

FIGURE 2 Adsorption isotherms for Ne as in Fig. 1.

The self-diffusivities for Ar and Ne in the SWNTs and silicalite are plotted in Figs. 3 and 4. Silicalite has a 3-D pore structure that allows anisotropic diffusion in the x, y and z directions. We here report only the orientationally averaged diffusivities [11,19], which are appropriate for describing randomly oriented polycrystalline silicalite membranes [51]. Note that D_s of Ne in silicalite is relatively constant over the entire range of pressures covered. This is partly due to the low loadings of Ne; a pressure of about 100 bar corresponds to 6 Ne atoms per unit cell, while for Ar in silicalite a 50 bar external pressure gives a loading of 12 atoms per unit cell. Hence, there are fewer adsorbate–adsorbate collisions for Ne than Ar in silicalite at the same bulk pressure and $D_s(c)$ does not decrease as fast as Ar in silicalite. Values of $D_s(c)$ for both Ar and Ne in all the nanotubes decrease dramatically with increased loading. As noted before [9], this is due to the smoothness of the nanotube potential energy surface, which results in the dominance of atom–atom collisions in momentum decorrelation as compared with atom–nanotube collisions. Hence, $D_s(c = 0)$ for Ar and Ne is about three orders of magnitude faster in the nanotubes compared with silicalite, whereas at the highest pressures diffusion is only about one order of magnitude faster in SWNTs. These results are also very similar to those observed previously for CH_4 and H_2 [9]. The D_s data for Ar in the different SWNTs are all qualitatively similar. The estimated uncertainties are smaller than the size of the symbols in the figures. There appears to be very little dependence of D_s on the diameter of the nanotube for the range of SWNT sizes studied here. In contrast, diffusion of Ne

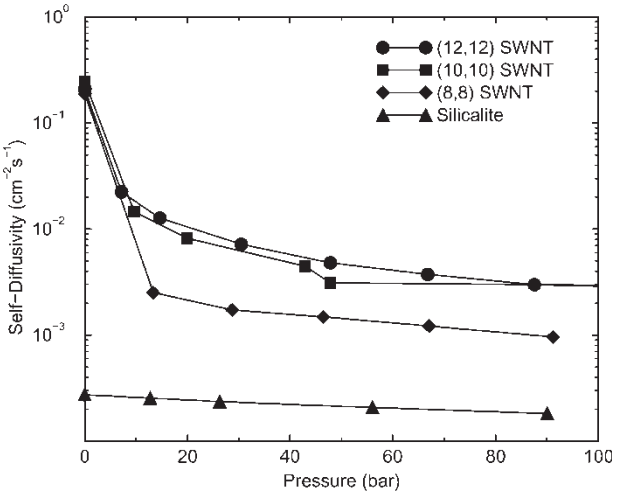

FIGURE 4 Self diffusivity of Ne as in Fig. 3.

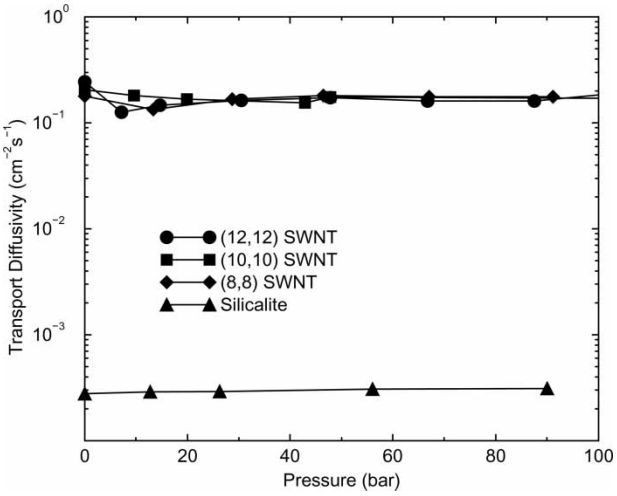

FIGURE 6 Transport diffusivity of Ne as in Fig. 5.

in the (8,8) nanotube appears to be significantly slower at high loadings than in the other nanotubes (see Fig. 4). This decrease of D_s with decreasing diameter is the opposite trend observed for H_2 [9].

Values of $D_t(c)$ for Ar and Ne are plotted in Figs. 5 and 6. The most striking feature of these figures is that D_t in the nanotubes is about a factor of 1000 larger in SWNTs than in silicalite, over the entire range of loadings. This is consistent with the behavior of CH_4 and H_2 in (10,10) nanotubes, silicalite, and ZSM-12 [9]. Note that $D_t(c)$ of Ar in silicalite increases with increasing loading, whereas Ar in the (10,10) and (12,12) SWNTs first decreases with increasing c and then increases slightly. This is because the initial momentum decorrelation introduced by adsorbate–adsorbate collisions manifested in D_s also leads to decreases in D_0 (not shown) and D_t at low concentrations. However, D_0 decreases only slightly with increasing concentration, changing by about a factor of three for the larger nanotubes. The thermodynamic correction factor, initially unity at low pressures, increases with increasing loading faster than $D_0(c)$ decreases at higher loadings. Hence, the initial decrease and subsequent increase in $D_t(c)$ is a result of the competing effects of adsorbate–adsorbate momentum decorrelation and the shape of the equilibrium adsorption isotherm. $D_0(c)$ in the (8,8) nanotube is almost constant and the thermodynamic correction factor increases very rapidly with c, making $D_t(c)$ a monatonically increasing function. All D_t values for Ne are relatively constant with pressure. This is partly due to the low concentrations of Ne in the sorbents. If the pressure were extended to much higher values then we believe behavior consistent with the Ar data reported in Fig. 5 would be observed.

The steady state fluxes of Ar and Ne through hypothetical membranes can be predicted from our D_t data and the adsorption isotherms, assuming negligible transport resistance at the membrane interfaces [51,52]. We have assumed membranes 10 μm thick constructed of polycrystalline silicalite or perfectly aligned SWNT with inter-tube gaps of 0.32 nm, consistent with the data in Figs. 1 and 2. The predicted fluxes are plotted in Fig. 7 for Ar and in Fig. 8 for Ne. Flux through membranes composed of (12,12) and (10,10) nanotubes are compared with flux through a silicalite membrane. A constant pressure drop of 1.38 bar is assumed across all the membranes. This pressure drop is typical for experimental membranes. The inlet pressure is varied to account for the variation of flux as a function of loading. This model has shown good agreement with experimentally measured CH_4 flux through polycrystalline silicalite membranes [51]. Flux through the SWNT membranes is predicted to be approximately four orders of magnitude higher than through silicalite.

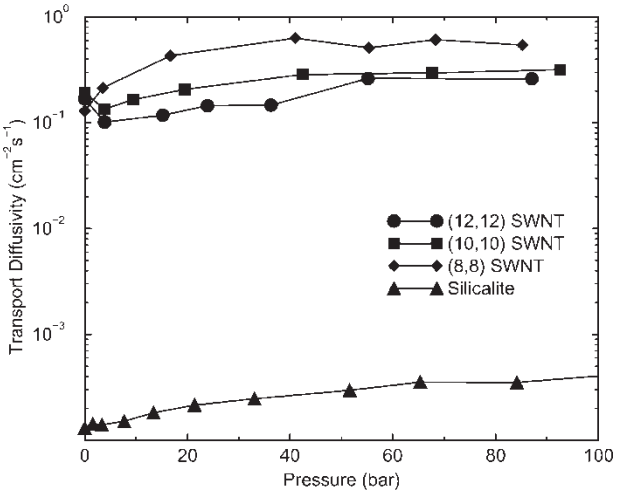

FIGURE 5 Transport diffusivity of Ar at 298 K in (12,12) (circles) (10,10) (squares) and (8,8) (diamonds) SWNTs and silicalite (triangles).

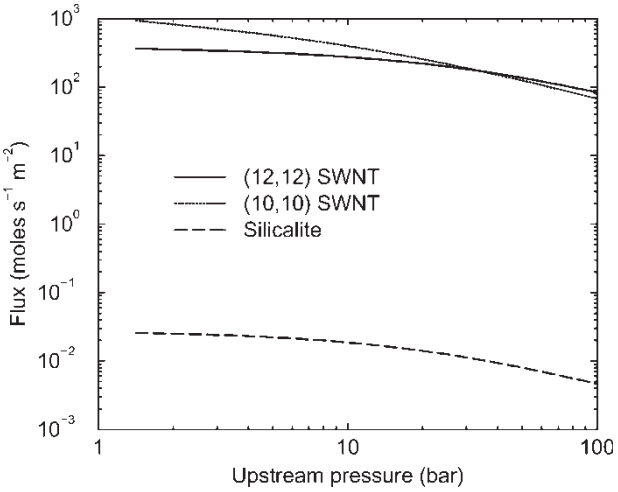

FIGURE 7 Predicted flux of Ar across a 10 μm thick membrane as a function of the upstream (inlet) pressure. The downstream (outlet) pressure is 1.38 bar lower than the upstream pressure. The solid line is for a (12,12) SWNT membrane, the dotted line is for a (10,10) SWNT membrane, and the dashed line is for a silicalite membrane.

In conclusion, we note that typical light gas diffusivities in gases, liquids and glassy polymers are 10^{-1}, 10^{-5} and 10^{-10}–$10^{-9}\,cm^2\,s^{-1}$, respectively [53,54]. Diffusivities inside crystalline microporous solids are sensitive functions of the adsorbent structure. For example, the diffusivity of CH_4 is roughly $10^{-4}\,cm^2\,s^{-1}$ in silicalite [9] but only $4 \times 10^{-11}\,cm^2\,s^{-1}$ in zeolite 4A [3]. In comparison, we observe that diffusion of small molecules through SWNTs is orders of magnitude faster than diffusion in any known microporous adsorbent and in fact is the same order of magnitude as diffusion in gases. Thus, SWNTs seem to represent the ideal limit for transport through microporous sorbents.

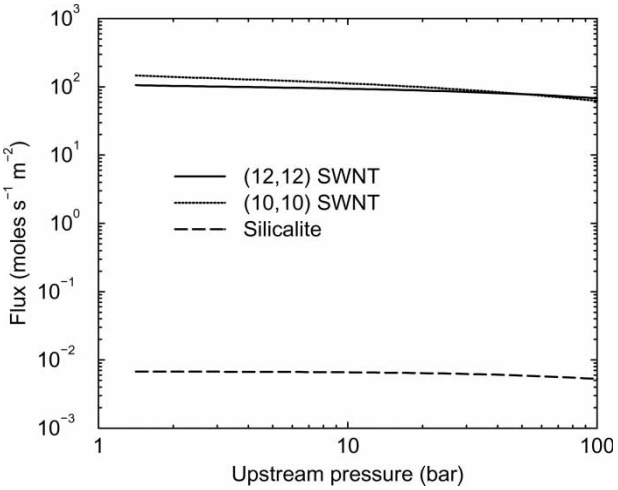

FIGURE 8 Predicted flux of Ne across a 10 μm thick membrane as a function of the upstream (inlet) pressure. Conditions are the same as in Fig. 7.

Acknowledgements

We acknowledge the National Science Foundation for support of this work under grant numbers #CTS-9983647 (DSS) #CTS-9702239 (JKJ). DMA is supported by the NSF REU program. DSS is an Alfred P. Sloan Fellow and a Camille Dreyfus Teacher-Scholar.

References

[1] Burggraaf, A., Vroon, Z., Keizer, K. and Verweij, H. (1998) "Permeation of single gases in thin zeolite MFI membranes", *J. Membr. Sci.* **144**, 77–86.
[2] Yang, R.T. (1997) *Gas separation by adsorption processes* (Imperial college Press, London).
[3] Käarger, J. and Ruthven, D.M. (1992) *Diffusion in Zeolites and Other Microporous Solids* (John Wiley and Sons, New York).
[4] Robeson, L.M. (1991) "Correlation of separation factor versus permeability for polymeric membranes", *J. Membr. Sci.* **62**, 165–185.
[5] Freeman, B.D. (1999) "Basis of permeability/selectivity tradeoff relations in polymeric gas separation membranes", *Macromolecules* **32**, 375–380.
[6] Koros, W.J., Fleming, G.K., Jordan, S.M., Kim, T.H. and Hoehn, H.H. (1988) "Polymeric membrane materials for solution-diffusion based permeation separations", *Prog. Polym. Sci.* **13**, 339–401.
[7] Strano, M.S., Zydney, A.L., Barth, H., Wooler, G., Agarwal, H. and Foley, H.C. (2002) "Ultrafiltration membrane synthesis by nanoscale templating of porous carbon", *J. Membr. Sci.* **198**, 173–186.
[8] Strano, M.S. and Foley, H.C. (2002) "Temperature- and pressure-dependent transient analysis of single component permeation through nanoporous carbon membranes", *Carbon* **40**, 1029–1041.
[9] Skoulidas, A.I., Ackerman, D.M., Johnson, J.K. and Sholl, D.S. (2002) "Rapid Transport of Gases in Carbon Nanotubes", *Phys. Rev. Lett.* **89**, 185901.
[10] Springer, T. (1972) In: Höhler, G., ed, *Quasielastic Neutron Scattering for the Investigation of Diffusive Motions in Solids and Liquids, Vol. 64 of Springer Tracts in Modern Physics* (Springer, Berlin).
[11] Skoulidas, A.I. and Sholl, D.S. (2002) "Transport diffusivities of CH_4, CF_4, He, Ne, Ar, Xe, and SF_6 in silicalite from atomistic simulations", *J. Phys. Chem. B* **106**, 5058–5067.
[12] Jobic, H., Kärger, J. and Bée, M. (1999) "Simultaneous measurement of self- and transport diffusivities in zeolites", *Phys. Rev. Lett.* **82**, 4260–4263.
[13] Ahunbay, M.G., Elliot, J.R. and Talu, O. (2002) "The diffusion process of methane through a silicalite single crystal membrane", *J. Phys. Chem. B* **106**, 5163–5168.
[14] Martin, M.G., Thompson, A.P. and Nenoff, T.M. (2001) "Effect of pressure, membrane thickness, and placement of control volumes on the flux of methane through thin silicalite membranes: a dual control volume grand canonical molecular dynamics study", *J. Chem. Phys.* **114**, 7174–7181.
[15] Heffelfinger, G.S. and Ford, D.M. (1998) "Massively parallel dual control volume grand canonical molecular dynamics with LADERA II Gradient driven diffusion in Lennard-Jones fluids", *Mol. Phys.* **94**, 673–684.
[16] Heffelfinger, G.S. and Van Swol, F. (1994) "Diffusion in Lennard-Jones fluids using dual control volume grand canonical molecular dynamics simulation (DCV-GCMD)", *J. Chem. Phys.* **100**, 7548–7552.
[17] Maginn, E.J., Bell, A.T. and Theodorou, D.N. (1993) "Transport diffusivity of methane in silicalite from equilibrium and nonequilibrium simulations", *J. Phys. Chem.* **97**, 4173–4181.
[18] Theodorou, D.N., Snurr, R.Q. and Bell, A.T. (1996) "Molecular dynamics and diffusion in microporous materials", In: Alberti, G. and Bein, T., eds, *Comprehensive Supramolecular Chemistry* (Pergamon Press, New York) **Vol. 7**, pp 507–548.

[19] Skoulidas, A.I. and Sholl, D.S. (2001) "Direct tests of the Darkin approximation for molecular diffusion in zeolites using equilibrium molecular dynamics", *J. Phys. Chem. B* **105**, 3151–3154.
[20] Keil, F.J., Krishna, R. and Coppens, M.O. (2000) "Modeling of diffusion in zeolites", *Rev. Chem. Eng.* **16**, 71–197.
[21] Auerbach, S.M. (2000) "Theory and simulation of jump dynamics, diffusion and phase equilibrium in nanopores, Int", *Rev. Phys. Chem.* **19**, 155–198.
[22] Iijima, S. (1991) "Helical Microtubules of Graphitic Carbon", *Nature* **354**, 56–58.
[23] Iijima, S. and Ichihashi, T. (1993) "Single-shell carbon nanotubes of 1-nm diameter", *Nature* **363**, 603–605.
[24] Bethune, D.S., Kiang, C.H., Vries, de M.S., Gorman, G., Savoy, R., Vazquez, J. and Beyers, R. (1993) "Cobalt-catalyzed growth of carbon nanotubes with single-atomic-layer walls", *Nature* **363**, 605–607.
[25] Peng, L.M., Zhang, Z.L., Xue, Z.Q., Wu, Q.D., Gu, Z.N. and Pettifor, D.G. (2000) "Stability of carbon nanotubes: how small can they be?", *Phys. Rev. Lett.* **85**, 3249–3252.
[26] Sun, L.F., Xie, S.S., Liu, W., Zhou, W.Y., Liu, Z.Q., Tang, D.S., Wang, G. and Qian, L.X. (2000) "Materials: creating the narrowest carbon nanotubes", *Nature* **403**, 384.
[27] Qin, L.-C., Zhao, X., Harahara, K., Miyamoto, Y., Ando, Y. and Iijima, S. (2000) "The smallest carbon nanotube", *Nature* **408**, 50.
[28] Wang, N., Tang, Z.K., Li, G.D. and Chen, J.S. (2000) "Single-walled 4 Å carbon nanotube arrays", *Nature* **408**, 50–51.
[29] Liang, W.Z., Chen, G.H., Li, Z. and Tang, Z.-K. (2002) "Absorption spectra and chirality of single-walled 4 Å carbon nanotubes", *Appl. Phys. Lett.* **80**, 3415–3417.
[30] Thess, A., Lee, R., Nikolaey, P., Dai, H., Petit, P., Robert, J., Xu, C., Lee, Y., Kim, S., Rinzler, A., Colbert, D., Scuseria, G., Tomanek, D., Fischer, J. and Smalley, R. (1996) "Crystilline ropes of metallic carbon nanotubes", *Science* **273**, 483–487.
[31] Zhu, H.W., Xu, C.L., Wu, D.H., Wei, B.Q., Vajtai, R. and Ajayan, P.M. (2002) "Direct synthesis of long single-walled carbon nanotube strands", *Science* **296**, 884–886.
[32] White, C.T., Robertson, D.H. and Mintmire, J.W. (1993) "Helical and rotational symmetries of nanoscale graphitic tubules", *Phys. Rev. B* **47**, 5485–5488.
[33] Nicholson, D. (2002) "A simulation study of the pore size dependence of transport selectivity in cylindrical pores", *Mol. Phys.* **100**, 2151–2163.
[34] Mao, Z., Garg, A. and Sinnott, S.B. (1999) "Molecular dynamics simulations of the filling and decorating of carbon nanotubules", *Nanotechnology* **10**, 273–277.
[35] Mao, Z. and Sinnott, S.B. (2000) "A computational studey of molecular diffusion and dynamic flow through carbon nanotubes", *J. Phys. Chem. B* **104**, 4618–4624.
[36] Mao, Z. and Sinnott, S.B. (2001) "Separation of organic molecular mixtures in carbon nanotubes and bundles: molecular dynamics simulations", *J. Phys. Chem. B* **105**, 6916–6924.
[37] Brenner, D.W., Shenderova, O.A., Harrison, J.A., Stuart, S.J., Ni, B. and Sinnott, S.B. (2002) "A second-generation reactive empirical bond order (REBO) potential energy expression for hydrocarbons", *J. Phys. Cond. Matt.* **14**, 783–802.
[38] Brenner, D.W. (2000) "The art and science of an analytic potential", *Phys. Status Solid B* **217**, 23–40.
[39] Sinnott, S.B., Qi, L., Shenderova, O.A. and Brenner, D.W. (1999) In: Hase, W., ed, *Molecular dynamics of clusters, surfaces, liquids, and interfaces* (JAI Press, Stanford, CT).
[40] Sokhan, V.P., Nicholson, D. and Quirke, N. (2001) "Fluid flow in nanopores: An examination of hydrodynamic boundary conditions", *J. Chem. Phys.* **115**, 3878–3887.
[41] Sokhan, V.P., Nicholson, D. and Quirke, N. (2002) "Fluid flow in nanopores: accurate boundary conditions for carbon nanotubes", *J. Chem. Phys.* **117**, 8531–8539.
[42] Tersoff, J. (1986) "New empirical model for the structural properties of silicon", *Phys. Rev. Lett.* **56**, 632–635.
[43] Brenner, D.W. (1990) "Empirical potential for hydrocarbons for use in simulating the chemical vapor deposition of diamond films", *Phys. Rev. B* **42**, 9458–9471.
[44] Düren, T., Kiel, F.J. and Seaton, N.A. (2002) "Composition dependent transport diffusion coefficients of CH_4/CF4 mixtures in carbon nanotube by non-equilibrium molecular dynamics simulations", *Chem. Eng. Sci.* **57**, 1343–1354.
[45] MacElroy, J.M.D. and Boyle, M.J. (1999) "Nonequilibrium molecular dynamics simulation of a model carbon membrane separation of CH_4/H_2 mixtures", *Chem. Eng. J.* **74**, 84–97.
[46] Steele, W.A. (1974) *The Interaction of Gases With Solid Surfaces* (Pergamon Press, Oxford).
[47] Schultz, M. (1973) *Spline Analysis* (Prentice-Hall, Englewood Cliffs, NJ).
[48] Allen, M.P. and Tildesley, D.J. (1987) *Computer Simulation of Liquids* (Clarendon, Oxford).
[49] Frenkel, D. and Smit, B. (2002) *Understanding Molecular Simulation From Algorithms to Applications*, 2nd Ed. (Academic Press, San Diego).
[50] Dymond, J.H. and Smith, E.B. (1969) *The Virial Coefficients of Gases—A Critical Compilation* (Clarendon Press, Oxford).
[51] Bowen, T.C., Falconer, J.L., Noble, R.D., Skoulidas, A.I. and Sholl, D.S. (2002) "A Comparison of Atomistic Simulations and Experimental Measurements of Light Gas Permeation through Zeolite Membranes", *Ind. Eng. Chem. Res.* **41**, 1641–1650.
[52] Sholl, D.S. (2000) "Predicting Single-Component Permeance through Macroscopic Zeolite Membranes from Atomistic Simulations", *Ind. Eng. Chem. Res.* **39**, 3737–3746.
[53] Cussler, E.L. (1976) *Multicomponent Diffusion* (Elsevier, Amsterdam).
[54] Greenfield, M.L. and Theodorou, D.N. (2001) "Coarse-grained molecular simulation of penetrant diffusion in a glassy polymer using reverse and kinetic Monte Carlo", *Macromolecules* **34**, 8541–8553.